GEOPHYSICS, VOL. 64, NO. 4 (JULY-AUGUST 1999); P. 1193–1201, 7 FIGS., 3 TABLES.

Fracture detection using azimuthal variation of *P*-wave moveout from orthogonal seismic survey lines

Xiang-Yang Li*

ABSTRACT

An algorithm is proposed for determining the fracture orientation based on the azimuthal variations in the *P*-wave reflection moveout for a target interval. The differential moveout between orthogonal survey lines from the bottom of a given target shows $\cos 2\phi$ variations with the line azimuth ϕ measured from the fracture strike for a fixed offset. A configuration of four intersecting survey lines may be used to quantify the fracture strike. The four lines form two orthogonal pairs, and the fracture strike can be obtained by analyzing the crossplot of the two corresponding pairs of the differential moveouts. An offset-depth ratio (x/z) of 1.0 or greater (up to 1.5) is often required to quantify the moveout difference reliably. The sensitivity of the method is further enhanced by low/high impedance contrast at the top target interface but is greatly reduced by high/low impedance contrast. The method may be particularly useful in marine exploration with repeated surveys of various vintages where continuous azimuthal coverage is often not available. A data set from the North Sea is used to illustrate the technique.

INTRODUCTION

Recently, the use of *P*-waves for fracture detection has attracted considerable interest. These include azimuthal *P*-wave amplitude versus offset (AVO) (Lefeuvre, 1994; Lynn et al., 1996; Mallick et al., 1996), azimuthal variations in *P*-wave NMO velocity (Sena, 1991; Corrigan et al., 1996; Tsvankin, 1997), and azimuthal variations in *P*-wave moveout (Li, 1997; Sayers and Ebrom, 1997). Of all these techniques, azimuthal NMO velocity analysis is most often used in the industry to determine fracture orientation.

In a medium containing fracture-induced transverse isotropy with a horizontal symmetry axis (HTI), the short-spread NMO velocity shows elliptical azimuthal variations, and the long axis of the NMO ellipse indicates the fracture strike. This feature was first recognized by Tsvankin (1995, 1997) and subsequently generalized to inhomogeneous anisotropic media by Tsvankin et al. (1997) and Grechka and Tsvankin (1998). In practice, careful data processing is required to minimize the error propagation and magnification through various processing steps (Al-Dajani and Alkahalifah, 1998), and this limits the application of the technique to some extent.

Here I present an alternative approach for determining the fracture orientation (strike) in HTI media. The approach is based on the traveltime (moveout) difference between two orthogonal survey lines for a fixed offset, referred to as the azimuthal moveout response (AMR). Assuming a fractured target embedded into a background of azimuthally isotropic media, I develop analytical expressions for quantifying the AMR from the fractured target. This leads to the development of a crossplotting algorithm for determining the fracture strike based on orthogonal seismic survey lines. Note that orthogonal 2-D (or even 3-D) seismic surveys were common in the industry, and these surveys were often repeated during various stages of oil-field development. The proposed method is applied to marine streamer data from repeated surveys of various vintages and is compared with the NMO velocity method for confirmation.

FRACTURE-INDUCED AZIMUTHAL ANISOTROPY

This section introduces the Thomsen parameters and the reflection moveout equation for fracture-induced HTI media, which are needed to derive the *P*-wave moveout difference between orthogonal survey lines.

Thomsen parameters

A medium containing aligned vertical penny-shaped fractures gives rise to HTI. Use v_{p0} and v_{s0} to denote the vertical velocities of the *P*-wave and the fast split shear wave, respectively. Under the natural coordinate system determined by the

Presented at the 67th Annual Meeting, Society of Exploration Geophysicists. Manuscript received by the Editor February 2, 1998; revised manuscript received January 11, 1999.
*British Geological Survey, Murchison House, West Mains Road, Edinburgh EH9 3LA, Scotland, U.K. E-mail: x.y.li@bgs.ac.uk.

fracture normal (x_1), strike (x_2), and vertical axis (x_3), with stiffness tensor C_{ij} and density ρ, the Thomsen parameters may be defined as

$$v_{p0} = \sqrt{\frac{C_{33}}{\rho}}; \qquad v_{s0} = \sqrt{\frac{C_{44}}{\rho}};$$
$$\epsilon = \frac{C_{33} - C_{11}}{2C_{11}}; \qquad \gamma = \frac{C_{44} - C_{66}}{2C_{66}}; \tag{1}$$
$$\delta = \frac{(C_{13} + C_{66})^2 - (C_{11} - C_{66})^2}{2C_{11}(C_{11} - C_{66})}.$$

These are generic Thomsen parameters defined with respect to the horizontal symmetry axis of the HTI medium. Comparing this definition for HTI with the original definition for vertical transverse isotropy (VTI) in Thomsen (1986), one notices an interchange of indices between 11 and 33, 44, and 66. This interchange is necessary to keep the quantities of Thomsen parameters of an HTI medium the same as in its equivalent VTI medium. An alternative way is to define effective Thomsen parameters with respect to the vertical axis, as described by Tsvankin (1997).

P-wave moveout equation in a single HTI layer

For a survey line at the azimuthal angle ϕ to the fracture strike of a single-layered HTI medium, the reflection moveout can be written as, following Sayers and Ebrom (1997),

$$t^2(\phi, x) = t_0^2 + \frac{x^2}{v_{\text{nmo}}^2} - \frac{Ax^4}{x^2 + t_0^2 v_{p0}^2}, \tag{2}$$

where $t(x, \phi)$ is the reflection traveltime at offset x, t_0 is the two-way zero-offset traveltime, v_{nmo} is the NMO velocity, and A is a moveout coefficient. Equation (2) is obtained for weak anisotropy (see also Sena, 1991; Li and Crampin; 1993); for general anisotropy, a more accurate equation is given in Al-Dajani and Tsvankin (1998). From Al-Dajani and Tsvankin (1998), v_{nmo} and coefficient A can be written, to the first order in the anisotropy parameters, as

$$\frac{1}{v_{\text{nmo}}^2} = \frac{1}{v_{p0}^2}[1 - 2(\delta - 2\epsilon)\sin^2\phi] \tag{3}$$

$$A = \frac{2(\epsilon - \delta)}{v_{p0}^2}\sin^4\phi. \tag{4}$$

The coefficient A satisfies $A = -t_0^2 v_{p0}^2 A_4$, where A_4 is the quartic moveout coefficient defined by Al-Dajani and Tsvankin (1998). Also, $\delta - 2\epsilon \approx \delta^{(V)}$ in the weak-anisotropy approximation, where $\delta^{(V)}$ is the effective Thomsen parameter from Tsvankin (1997).

Substituting equations (3) and (4) into equation (2), we take the square root and linearize with respect to the anisotropic parameters ϵ and δ:

$$t(\phi, x) = \sqrt{t_0^2 + \frac{x^2}{v_{p0}^2}}[1 - (\delta - 2\epsilon)\sin^2\theta\sin^2\phi - (\epsilon - \delta)\sin^4\theta\sin^4\phi], \tag{5}$$

where θ is the incidence (ray) angle at the reflector measured from vertical and the square root term in equation (5) is a standard NMO term.

Introducing $t_\parallel$ and $t_\perp$ as the reflection moveouts at offset x for the survey lines parallel and perpendicular to the fracture strike, respectively, leads to

$$t_\parallel(x) = t(\phi = 0, x) = \sqrt{t_0^2 + \frac{x^2}{v_{p0}^2}}; \tag{6}$$

$$t_\perp(x) = t(\phi = \pi/2, x) = t_\parallel(x) - t_\parallel(x)(\delta - 2\epsilon)\sin^2\theta - t_\parallel(x)(\epsilon - \delta)\sin^4\theta. \tag{7}$$

Substituting equations (6) and (7) into equation (5) yields

$$t(\phi, x) = t_\parallel(x)\cos^2\phi + t_\perp(x)\sin^2\phi + t_\parallel(x)(\epsilon - \delta)\sin^4\theta\sin^2\phi\cos^2\phi. \tag{8}$$

ANALYSIS OF AZIMUTHAL MOVEOUT RESPONSE

Here I consider two cases: (1) a single fractured HTI layer and (2) multilayered HTI media with a uniform fracture orientation. The latter can be a fractured layer (the target) embedded either into an azimuthally isotropic background or into a fractured HTI background which has the same fracture strike as the target. In both cases, there is a fixed fracture-strike azimuth. The more general case of multilayered fractured HTI media with arbitrary fracture orientations is discussed in the Appendix.

I assume two orthogonal common midpoint (CMP) lines at azimuths ϕ and $\phi + \pi/2$ measured from the fixed fracture strike. The AMR of a fracture target is defined as the traveltime difference (Δt) between the two orthogonal lines from the bottom of the target:

$$\Delta t(\phi, x) = t(\phi + \pi/2, x) - t(\phi, x). \tag{9}$$

As shown in equation (5), the traveltime equation explicitly contains the square root moveout term. It is thus more convenient to apply a common hyperbolic moveout correction to both azimuthal lines before calculating Δt. This implies rearranging equation (9) as

$$\Delta t(\phi, x) = \left[t(\phi + \pi/2, x) - \sqrt{t_0^2 + \frac{x^2}{v_{mo}^2}}\right] - \left[t(\phi, x) - \sqrt{t_0^2 + \frac{x^2}{v_{mo}^2}}\right], \tag{10}$$

where v_{mo} is the picked moveout velocity.

Analytical approximations for Δt

Single HTI layer.—From equation (8), Δt can be written as

$$\Delta t(\phi, x) = (t_\perp - t_\parallel)\cos 2\phi = B_0(x, \epsilon, \delta)\cos 2\phi, \tag{11}$$

where, to the first order in the anisotropy parameters,

$$B_0(x, \epsilon, \delta) = \frac{x}{v_{p0}}\sin\theta[2\epsilon - \delta - (\epsilon - \delta)\sin^2\theta]. \tag{12}$$

Since $B_0(x, \epsilon, \delta)$ is independent of azimuth, equation (11) shows that in the weak-anisotropy approximation, the AMR is a function of $\cos 2\phi$ for a fixed offset.

Multilayered media with a single fracture orientation.—Assume the target fractured layer is the nth layer in a stratified medium. As shown in equation (A-15) in the Appendix, Δt can still be written as

$$\Delta t(\phi, x) = (t_\perp - t_\parallel)\cos 2\phi = B(x, \epsilon, \delta)\cos 2\phi. \quad (13)$$

If the target layer is embedded into an azimuthally isotropic background, $B(x, \epsilon, \delta)$ is evaluated locally at the fractured target:

$$B(x, \epsilon, \delta) = B_n = \frac{2x_{\parallel n}}{v_{p0n}} \sin\theta_{\parallel n}\left[2\epsilon - \delta - (\epsilon - \delta)\sin^2\theta_{\parallel n}\right], \quad (14)$$

where

$$\sin\theta_{\parallel n} = \frac{x_{\parallel n}}{\sqrt{t_{0n}^2 v_{p0n}^2 + x_{\parallel n}^2}}. \quad (15)$$

The value $x_{\parallel n}$ is the horizontal component of the ray segment within the fracture target, and $\theta_{\parallel n}$ is the incidence ray angle in the target; both are evaluated for the azimuth parallel to the fracture strike. The value t_{0n} is the zero-offset one-way interval time, and v_{p0n} is the interval vertical velocity in the fractured layer.

If there is more than one HTI layer, $B(x, \epsilon, \delta)$ is the sum of the components in all HTI layers, as shown in the Appendix. Again, since B is independent of azimuth in the weak-anisotropy approximation, equation (13) shows that the AMR in multilayered media with uniform fracture orientation is also a function of $\cos 2\phi$ for fixed offset. This feature allows us to determine the fracture strike without the need to know the ray-segment components. However, to invert for the anisotropy parameters using this method, ray tracing is needed to determine the ray-segment components.

Sensitivity of Δt

As an example, I consider a two-layer model with a fractured HTI target overlain by an isotropic overburden. I select three types of models with the parameters listed in Table 1. The first model is claystone (overburden) over fractured chalk (target) with low/high impedance contrast; the second is limestone over fractured chalk with a weak impedance contrast; and the third is shale over fractured gas sand with high/low impedance contrast. In all three models, the fractured layer occurs at 1500 m depth and has a thickness of 300 m and 10% fracture anisotropy (crack density = 0.1).

Azimuthal variations.—To evaluate the azimuthal variation, I fix the offset at $x = 3000$ m; then I calculate and display Δt for all azimuths for the three models using full-wave modeling, as shown in Figure 1a. The results confirm the prediction of equation (13), which agrees with the experimental results of Garotta (1989).

Impedance contrast at the top of the target.—Strong low/high or high/low impedance will cause ray bending and has significant effect on the moveout response. I select the orthogonal azimuths parallel and perpendicular to the fracture strike to maximize the effects and calculate Δt for a number of offsets for the models in Table 1. A strong low/high impedance contrast enhances the sensitivity of the azimuthal response (dotted line, Figure 1b), while a strong high/low contrast reduces the sensitivity of the response (dashed line, Figure 1b). The case of weak contrast is between the previous two (solid line, Figure 1b).

Offset-depth ratio.—The sensitivity of AMR increases with offset in general, with either enhanced or reduced sensitivity because of variations in impedance contrast. As shown in

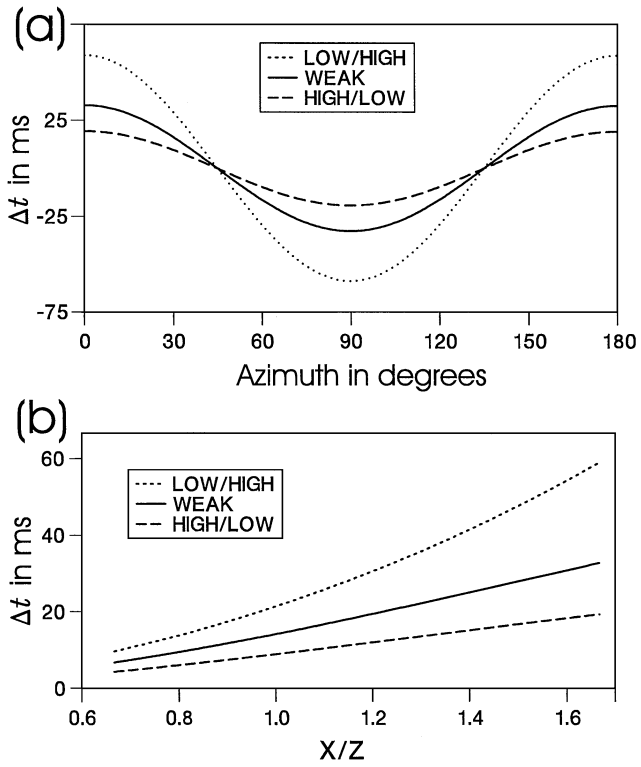

FIG. 1. Variations of AMR for the three models from Table 1. (a) Variations with azimuth at constant offset $x = 3000$ m; (b) variations with offset-depth ratio (x/z) of the moveout difference calculated between the two azimuths parallel (0°) and perpendicular (90°) to the fracture strike.

Table 1. Parameters of the three models used in the study.

Models		Density (g/cm^3)	v_{p0} (m/s)	v_{s0} (m/s)	ϵ	δ	γ	Thickness (m)
Model 1: low/high (claystone/chalk)	Layer 1	1.97	2400	1100	0	0	0	1500
	Layer 2	2.5	3500	1750	0.26	0.18	0.12	300
Model 2: weak (limestone/chalk)	Layer 1	2.5	3640	1750	0	0	0	1500
	Layer 2	2.5	4000	2000	0.26	0.18	0.12	300
Model 3: high/low (shale/gas sand)	Layer 1	2.3	3048	1574	0	0	0	1500
	Layer 2	2.19	2183	1502	0.27	0.26	0.15	300

Figure 1b, to develop a 20-ms difference in the interval variation for model 1 with low/high impedance, we need an offset-depth ratio (x/z) of 1.0. For model 2 with weak impedance and model 3 with high/low impedance, the required values of x/z are 1.2 and >1.6, respectively.

Acquisition design and processing algorithms

Special four-line configuration with 45° separation.—Consider four intersecting survey lines with 45° separation (Figure 2a). The four lines can be arranged into two orthogonal sets. Denote the AMR for the first set as $\Delta t_1(\phi, x)$ and the second set as $\Delta t_2(\pi/4 - \phi, x)$. Note that in Figure 2a positive ϕ represents a counterclockwise rotation from line 1 to the fracture strike. This is consistent with the 2-D rotation convention under a right-handed coordinate system with the third axis pointing to the reader. Using equation (13) gives

$$\Delta t_1(\phi, x) = \Delta t(\phi, x) = B \cos 2\phi$$

and

$$\Delta t_2(\pi/4 - \phi, x) = B \sin 2\phi,$$

which leads to

$$\tan 2\phi = \frac{\sin 2\phi}{\cos 2\phi} = \frac{\Delta t_2(\pi/4 - \phi, x)}{\Delta t_1(\phi, x)}. \qquad (16)$$

This implies that the crossplot of $\Delta t_1(\phi,\ x)$ versus $\Delta t_2(\pi/4 - \phi,\ x)$ for the four-line configuration in Figure 2a will show a linear trend determined by the angle of 2ϕ to the $\Delta t_1(\phi,\ x)$ axis. This axis represents the direction of line 1 in Figure 2a. Thus, a special four-line configuration allows a simple way to determine the fracture strike using crossplot analysis.

Special four-line configuration with arbitrary separation.—The two orthogonal sets in the previous configuration are separated by 45°. Here I consider a case where the four lines also form orthogonal sets but are separated by an arbitrary angle φ_0 (Figure 2b). It follows that

$$\Delta t_1 = \Delta t(\phi, x) = B \cos 2\phi$$

and

$$\Delta t_2 = \Delta t(\varphi_0 - \phi, x) = B \cos 2(\varphi_0 - \phi),$$

which leads to

$$\Delta t_2' = B \sin 2\phi = (\Delta t_2 - \cos 2\varphi_0 \Delta t_1)/\sin 2\varphi_0 \qquad (17)$$

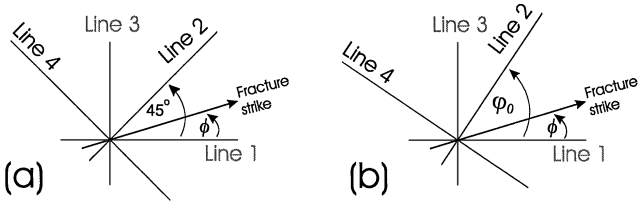

FIG. 2. Four-line configuration: (a) 45° separation; (b) separation by angle φ_0. Lines 1 and 3 form a right-handed coordinate system, with the third axis pointing to the reader. The value ϕ is the angle between line 1 and the fracture strike; positive ϕ indicates a counterclockwise rotation, while negative ϕ indicates a clockwise rotation.

and

$$\tan 2\phi = \sin 2\phi/\cos 2\phi = \Delta t_2'/\Delta t_1. \qquad (18)$$

Thus, for the four-line configuration in Figure 2b, after correcting Δt_2 using equation (17), the crossplot of Δt_1 versus $\Delta t_2'$ still shows a linear trend, indicating the direction of 2ϕ to the axis of Δt_1. Again, this axis represents the direction of line 1 in Figure 2b.

Since only the moveout difference between two orthogonal seismic lines shows the $\cos 2\phi$ variation, a minimum of two pairs of orthogonal lines is required to estimate the fracture strike. This is a shortcoming of the proposed technique compared with azimuthal NMO velocity analysis.

Angle definition and mapping.—Use ϕ_0 to denote the direction of the linear trend to the Δt_1 axis. Using equation (18) gives

$$\phi_0 = 2\phi = \begin{cases} \tan^{-1}\dfrac{\Delta t_2'}{\Delta t_1} & \text{if } \Delta t_1 > 0; \\ \tan^{-1}\dfrac{\Delta t_2'}{\Delta t_1} + \pi & \text{if } \Delta t_1 < 0 \text{ and } \Delta t_2' > 0\,, \\ \tan^{-1}\dfrac{\Delta t_2'}{\Delta t_1} - \pi & \text{if } \Delta t_1 < 0 \text{ and } \Delta t_2' < 0 \end{cases} \qquad (19)$$

where the main ranges of ϕ_0 are $(-\pi, \pi)$ and the axes of Δt_1 and $\Delta t_2'$ form a right-handed coordinate system with the third axis pointing to the reader. The value ϕ_0 is positive if the linear trend is in quadrants I and II ($\Delta t_2' > 0$) and negative if it is in quadrants III and IV ($\Delta t_2' < 0$). Once ϕ_0 is determined, the fracture strike ϕ is determined as $\phi = \phi_0/2$.

With the above angle definition, the determined fracture strike from the crossplot can be mapped into the survey lines in Figure 2 by analogy with the axis of Δt_1 in the crossplot to the direction of line 1 in the acquisition system—positive angle indicating a counterclockwise rotation and negative angle indicating a clockwise rotation (Figure 2).

Least-squares crossplot analysis.—Several different schemes of least-square analysis can be applied to the crossplot. Care should be taken to resolve the nonuniqueness of the inverse tangent function. Here I give two examples. The first one is linear regression, which yields

$$\phi_0 = \tan^{-1}\left\{\frac{\sum_x \Delta t_1 \Delta t_2'}{\sum_x \Delta t_1^2}\right\} \pm \pi. \qquad (20)$$

The summation is over all offsets, and the nonuniqueness can be resolved in the same manner as in equation (19). The second scheme is to minimize one of the coordinates by rotating the axes of Δt_1 and $\Delta t_2'$, which yields

$$\phi_0 = \frac{1}{2}\tan^{-1}\left\{\frac{2\sum_x \Delta t_1 \Delta t_2'}{\sum_x (\Delta t_1^2 - \Delta t_2'^2)}\right\} \pm \frac{n\pi}{2}, \quad n = 1, 2. \qquad (21)$$

For this scheme, the nonuniqueness can only be resolved by interactively checking the crossplot to see which quadrant the linear trend is located in.

APPLICATION AND RESULTS

The above algorithm is first applied to full-wave synthetic data for examining the accuracy of the method. This is followed by a field data example from the North Sea.

Synthetic tests

A 3000-m spread with 100-m receiver interval is used to construct full-wave synthetics, and five CDP gathers are calculated over five azimuthal lines for model 3 in Table 1 using the ANISEIS package based on the reflectivity method (Taylor, 1996). The model consists of a fractured gas sand overlain by an azimuthally isotropic shale overburden. Figure 3 shows the CDP gathers after moveout correction using the velocity for the line parallel to the fracture strike (0°), which is also used as a reference.

As shown in Figure 3, lines 1, 2, 3, and 4 (azimuth = 15°, 60°, 105°, and 150°) form two orthogonal sets. The first set is represented by $\phi = 15°$, the second by $\phi = 60°$. The residual moveouts of the bottom event at 1.25 s are picked interactively at the trough for all four lines, and the picked results are shown in Table 2. Note that the bottom event at line 1 is almost flat, while the bottom events at other lines are undercorrected. This indicates line 1 is close to the fracture strike because the NMO velocity parallel to the fracture strike is faster than the velocity perpendicular to the strike, and undercorrection occurs only when a faster NMO velocity is used.

Next, I examine the accuracy of equation (13), for it forms the basis of the analysis method. From the picked results in Table 2, the AMRs are calculated for lines 1 and 3: $\Delta t_1(15°, x) =$ line 3 − line 1. For lines 2 and 4, $\Delta t_2(60°, x) =$ line 4 − line 2. The results are displayed in Figure 4a; the triangles stand for $\Delta t_1(15°, x)$, the circles stand for $\Delta t_2(60°, x)$. The values $\Delta t_1(15°, x)$ and $\Delta t_2(60°, x)$ can also be calculated using the analytical equations (13) and (14), and they are displayed as solid lines in Figure 4a for comparison. The picked results from the CDP gathers in Figure 3 match the analytical results calculated from equation (13) very well for each corresponding offset and azimuth with an error <1%.

Then I examine the crossplot. Figure 4b shows the crossplot of $\Delta t_1(15°, x)$ versus $\Delta t_2(60°, x)$, and it reveals a linear trend in the direction of −30° from the axis of $\Delta t_1(15°, x)$. According to the angle convention, the axis of $\Delta t_1(15°, x)$ represents the direction of line 1. Thus, the crossplot confirms that the fracture strike is at −15° to line 1 (a clockwise rotation, Figure 4c).

To sum up, the full-wave modeling results confirm that equation (13) provides an accurate estimate of the AMR for a fractured layer. The analysis of the picked moveouts in Table 2

Table 2. Picked moveouts for the event at 1.25 s in Figure 3.

	t_{bottom} (ms)			
Offset (m)	Line 1	Line 3	Line 2	Line 4
0	1252	1252	1252	1252
100	1252	1252	1252	1252
200	1252	1252	1252	1252
300	1252	1252	1252	1252
400	1252	1252	1252	1252
500	1252	1252	1252	1252
600	1252	1253	1252	1252
700	1252	1253	1253	1252
800	1252	1253	1253	1252
900	1252	1254	1253	1252
1000	1252	1254	1253	1252
1100	1252	1254	1254	1252
1200	1252	1255	1254	1252
1300	1252	1255	1255	1253
1400	1252	1256	1255	1253
1500	1252	1256	1255	1253
1600	1252	1257	1256	1253
1700	1252	1257	1256	1253
1800	1252	1258	1256	1253
1900	1252	1258	1257	1253
2000	1252	1259	1257	1253
2100	1252	1259	1258	1253
2200	1251	1260	1258	1253
2300	1251	1261	1259	1253
2400	1251	1261	1259	1253
2500	1251	1262	1259	1253
2600	1251	1262	1260	1253
2700	1251	1263	1260	1253
2800	1250	1263	1260	1253
2900	1250	1263	1261	1253

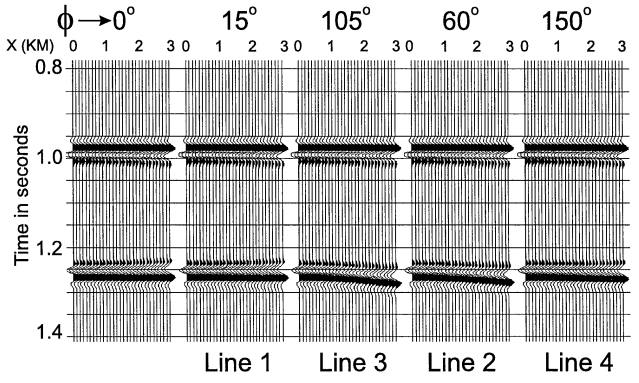

FIG. 3. CDP gathers for five different azimuths calculated for the shale/fractured gas sand model (model 3 in Table 1) with a high/low impedance contrast.

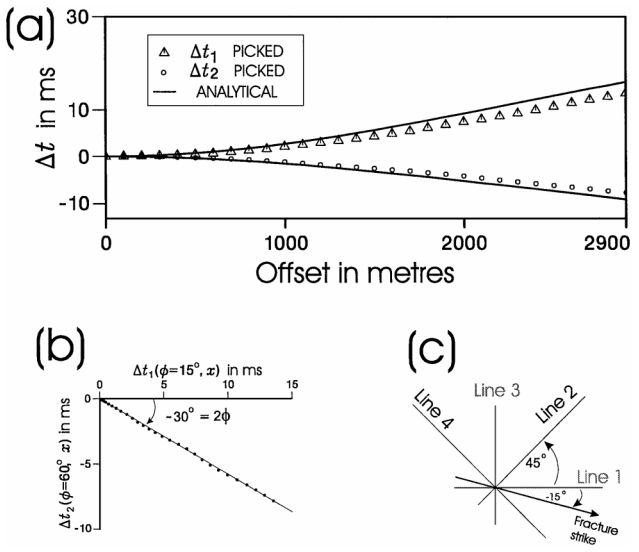

FIG. 4. (a) Comparison of the moveouts picked from Figure 3 with those calculated using equation (13) for model 3 in Table 1. (b) The crossplot of $\Delta t_1(15°, x)$ versus $\Delta t_2(60°, x)$. (c) The relationship between the fracture strike and the survey lines.

confirms the linear trend implied by equation (16), and the estimated fracture strike of -15° agrees with the actual value.

Field data example

The method is applied to a data set from the Fife field in the North Sea. The primary reservoir in the Fife field is the Upper Jurassic sandstone at a subsea depth of 2508 m. However, additional hydrocarbons have been encountered in the Upper Cretaceous chalk group above the sandstone at a depth of 2000 m, and the chalk was known to be fractured. Above the chalk is a massive isotropic thick claystone with very little lateral velocity variation (MacKertich, 1996). The chalk is about 200 m thick and allows sufficient separation of top and bottom chalk reflections, and the claystone/chalk interface with low/high impedance contrast enhances the sensitivity of the AMR. This geological setting is almost ideal for testing fracture detection using P-waves.

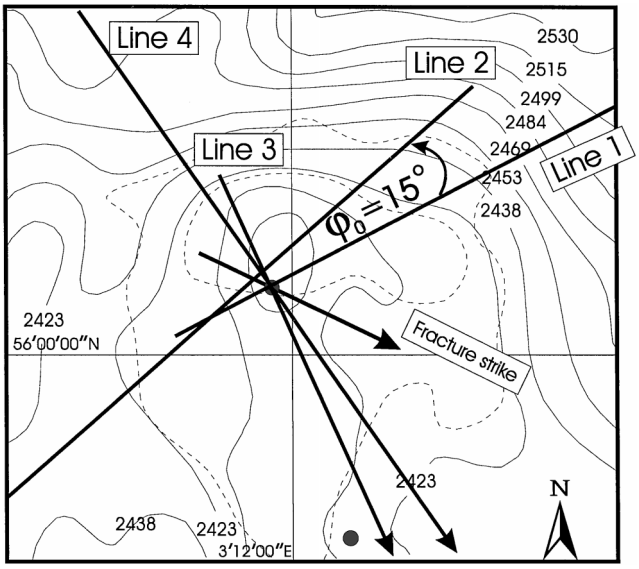

FIG. 5. Field data example. Map of the four seismic lines from the North Sea. Lines 1 and 3 intersect each other at CDPs 420 (line 1) and 440 (line 3), while lines 2 and 4 intersect at 730 (line 2) and 830 (line 4).

The data set consists of four intersecting lines from different vintages. Figure 5 shows the location and directions of the four seismic lines. Lines 1 and 3 were acquired in 1992 with an air gun source; lines 2 and 4 were acquired in 1982 with a water gun source. All four lines were shot at every station with a standard 3-km streamer and recorded with 120 channels. The station interval is 25 m. The initial offset for lines 1 and 3 is 121 m, and the initial offset for lines 2 and 4 is 185 m. Wavelet shaping was applied to the data to remove the inconsistency in the source signature.

The four lines form two orthogonal pairs separated by about 15°. Lines 1 and 3 (the first orthogonal set) intersect each other at CDPs 420 (line 1) and 440 (line 3); lines 2 and 4 (the second orthogonal set) intersect each other at CDPs 730 (line 2) and 830 (line 4). The two intersecting points of the two orthogonal sets are separated by about 20 CDPs (250 m) along lines 3 and 4.

Figure 6 shows the four CDP gathers after moveout correction using the same moveout velocity from the intersecting points of the four lines. A velocity function derived from line 2 was used for NMO corrections for all four lines. The top chalk corresponds to a peak and the bottom corresponds to a trough, and the two events are separated by about 100 ms two-way time. The top chalk event is almost flat after moveout correction (Figure 6), as expected. However, only in line 2 is the bottom chalk event flat, and in all other lines it is overcorrected. This indicates line 2 is close to the fracture normal because overcorrection only occurs when a slower velocity close to the fracture normal is used for NMO correction.

Interactive picking is adopted to track both the top and bottom chalk events. To minimize inconsistency resulting from picking, all traces are picked through troughs. The picked

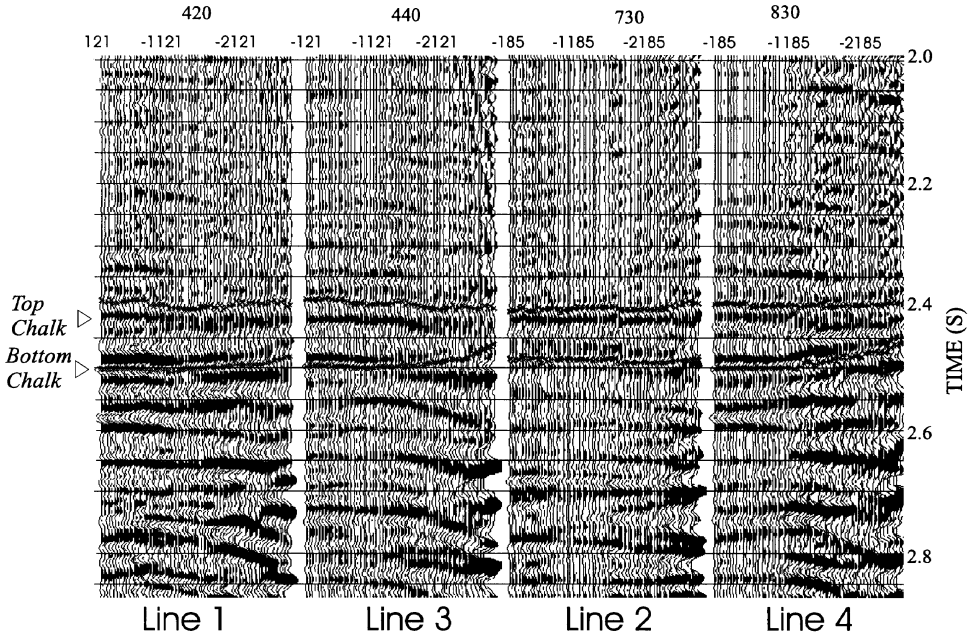

FIG. 6. The CDP gathers at the intersecting points of the four lines in Figure 5.

results beyond offset 2200 m are unreliable and are not included in the analysis because the amplitude of the bottom chalk event decreases with offset (see CDP 440, line 3).

After the picking, the processing steps can be summarized as follows:

1) Remove any residual statics resulting from the overburden by taking the interval moveout for all four azimuths from the picks in Figure 6 and further subtract the zero-offset interval time from the interval moveout to compensate for any inconsistency in location which may cause the near-offset moveout to vary;
2) Calculate the AMRs for the two orthogonal sets: $\Delta t_1(x) =$ line 3 $-$ line 1 and $\Delta t_2(x) =$ line 4 $-$ line 2;
3) Interpolate $\Delta t_2(x)$ through offsets so the offsets of the two sets match each other;
4) Calculate $\Delta t_2'(x)$ from $\Delta t_2(x)$ by applying equation (17); and
5) Crossplot $\Delta t_2'$ versus Δt_1 and apply equation (20) to determine the direction of the linear trend.

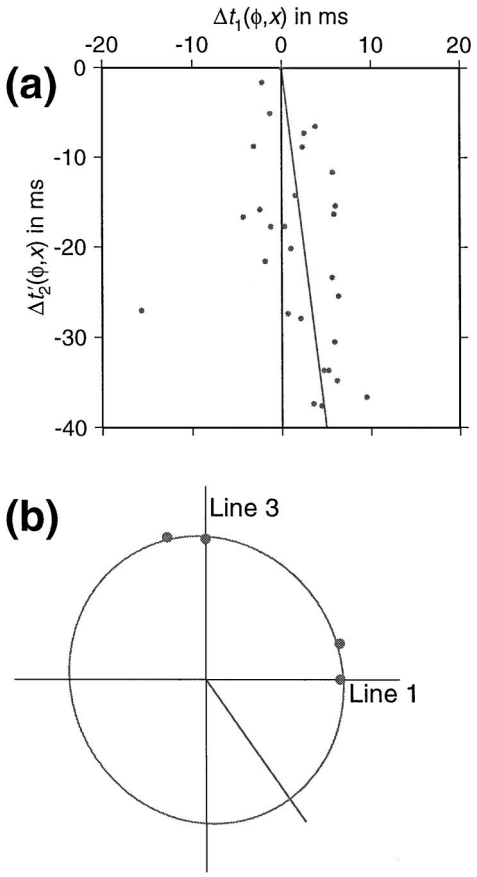

FIG. 7. (a) Crossplot of $\Delta t_1(x)$ versus $\Delta t_2'(x)$ obtained from Figure 6. (b) The interval NMO ellipse built from Table 3. The long axis is 3782 m/s, and the short axis is 3516 m/s with about 10% change.

Figure 7a shows the final crossplot from step 5, which reveals a trend close to the $\Delta t_2'$ axis. The angle calculated using equation (20) is -86° to the Δt_1 axis. Using the angle definition in Figure 2, this indicates the fracture strike is at -43° to line 1, which agrees with the strike of the local structure (Figure 5). In general, line 2 is close to the fracture normal and line 4 is close to the fracture strike. This result also agrees the analysis of the NMO-corrected gathers discussed previously (Figure 6) and with the AVO studies in MacBeth and Li (1999). The standard deviation of the linear trend in the crossplot may be used to access the quality of the final estimates. As shown in Figure 7a, the crossplot shows a good linear trend and there is no substantial deviation.

For comparison, Figure 7b shows the interval NMO ellipse built from the stacking velocities in Table 3. Different NMO velocities were used for different lines to flatten the bottom chalk event. The long axis is at -55° from line 1 and is close to the -43° angle from the crossplot. The long and short axes show a change of about 10%.

To sum up, despite some inconsistency in acquisition, the real data example confirms that crossplot analysis of moveout difference from orthogonal lines is a viable technique for detecting the fracture strike from marine streamer data of various vintages. Care must be taken to eliminate unreliable picks of moveouts at far offsets. Prior knowledge of the overburden and target is also essential. Careful velocity analysis and moveout correction are required to ensure that the event corresponding to the top of the target interval is properly aligned. The same velocity function should be applied to all four lines to preserve the azimuthal moveout variations.

DISCUSSION AND CONCLUSIONS

There are noticeable pitfalls in current *P*-wave techniques for fracture detection using amplitude behavior, particularly when applied to marine seismic data. Amplitude variation is very subtle and difficult to analyze in marine streamer data, where there is in general a lack of azimuthal coverage. To compensate for this, one must rely on repeated surveys of various vintages. For this kind of data, there are wide variations in acquisition conditions. A lot of effort must be placed on wavelet shaping and matching to make amplitude analysis possible.

The use of azimuthal moveout difference between two orthogonal lines shows potential in overcoming some of these problems. The method has good flexibility in handling irregular acquisition conditions because of the differential procedures used, as demonstrated in the real data example. This includes inconsistency in source signatures, offset and azimuthal sampling, and spatial variation of intersecting points. The final crossplot analysis reduces error propagation, makes the

Table 3. Picked NMO velocities for the field data in Figure 6. The two-way time t_0 is in ms, and NMO velocity v_{nmo} is in m/s.

Event	Line 1		Line 2		Line 3		Line 4	
	t_0	v_{nmo}	t_0	v_{nmo}	t_0	v_{nmo}	t_0	v_{nmo}
Top	2389	2130	2407	2130	2388	2130	2395	2130
Bottom	2503	2210	2484	2190	2497	2220	2502	2230
Interval v_{nmo}	114	3487	77	3591	109	3675	107	3838

method relatively robust, and allows for possible small errors during the various processing stages. However, the method does require special configuration of survey lines and wide-offset coverage with offset-depth ratio up to 1.0 for low/high impedance contrast and 1.5 for high/low impedance.

In conclusion, assuming a multilayered HTI model with uniform fracture orientation, I have obtained an approximate equation to calculate the differential moveout between two orthogonal survey lines [equation (13)]. The equation quantifies the effects of various factors—offset-depth ratio, impedance contrast, and layer thickness—and can help determine the sensitivity of the AMR. I have also presented a viable processing technique for determining the fracture strike based on a configuration of four intersecting survey lines. The four lines form two orthogonal pairs, and the fracture strike can be obtained by analyzing the crossplot of the two corresponding pairs of AMR. The method may be particularly useful for marine exploration where continuous azimuthal coverage is often not available.

ACKNOWLEDGMENTS

I thank the acting editor Ilya Tsvankin for his constructive comments on improving the manuscript and Thomas Kühnel for help with Latex. I thank the partners in the LINK project (Colin MacBeth and Frank Ohlsen of BGS, Wayne Kirk of Amerada Hess, Helmut Jakubowicz of Ensign) for the use of the real data. This work is published with the approval of the Director of the British Geological Survey (NERC) and the sponsors of EAP: AGIP, Amerada Hess, BP Amoco, BG plc, Chevron, Conoco, Elf, Fina, Mobil, PGS, Phillips, Saga Petroleum, Schlumberger, Shell, Texaco, and Veritas DGC.

REFERENCES

Al-Dajani, A., and Alkahalifah, T., 1998, Reflection moveout inversion in azimuthally anisotropic media—accuracy and limitations: 60th Internat. Mtg., Euro. Assoc. Geosci. Eng., Expanded Abstracts, 5–22.
Al-Dajani, A., and Tsvankin, I., 1998, Nonhyperbolic reflection moveout for horizontal transverse isotropy: Geophysics, **63**, 1738–1753.
Corrigan, D., Withers, R., Darnall, J., and Skopinski, T., 1996, Fracture mapping from azimuthal velocity analysis using 3D surface seismic data: 66th Ann. Internat. Mtg., Soc. Expl. Geophys., Expanded Abstracts, 1834–1837.
Garotta, R., 1989, Detection of azimuthal anisotropy: 59th Ann. Internat. Mtg., Soc. Expl. Geophys., Expanded Abstracts, 861–863.
Grechka, V., and Tsvankin, I., 1998, 3-D description of normal moveout in anisotropic in homogeneous media: Geophysics **63**, 1079–1092.
Lefeuvre, F., 1994, Fracture related anisotropy detection and analysis: "and if the *P*-waves were enough?" 64th Ann. Internat. Mtg., Soc. Expl. Geophys., Expanded Abstracts, 942–945.
Li, X.-Y., 1997, Viability of azimuthal variation in *P*-wave moveout for fracture detection: 67th Ann. Internat. Mtg., Soc. Expl. Geophys., Expanded Abstracts, 1555–1558.
Li, X.-Y., and Crampin, S., 1993, Approximations to shear-wave velocity and moveout equations in anisotropic media: Geophys. Prosp., **41**, 833–857.
Lynn, H. B., Simon, K. M., Bates, C. R., and Van Dok, R., 1996, Naturally fractured gas reservoir's seismic characterization: 66th Ann. Internat. Mtg., Soc. Expl. Geophys., Expanded Abstracts, 1360–1363.
MacBeth, C., and Li, X.-Y., 1999, AVD—An emerging new marine technology for reservoir characterization: Acquisition and application: Geophysics, **64**, 1153–1159, this issue.
MacKertich, D., 1996, The Fife field, UK central North Sea: Petro. Geoscience, **2**, 373–380.
Mallick, S., Craft, K. L., Meister, L. J., and Chambers, R. E., 1996, Computation of principal directions of azimuthal anisotropy from *P*-wave seismic data: 66th Ann. Internat. Mtg., Soc. Expl. Geophys., Expanded Abstracts, 1862–1865.
Sayers, C. M., and Ebrom, D. A., 1997, Seismic traveltime analysis for azimuthally anisotropic media: Theory and experiment: Geophysics, **62**, 1570–1582.
Sena, A. G., 1991, Seismic traveltime equations for azimuthally anisotropic and isotropic media: Estimation of interval elastic properties: Geophysics, **56**, 2090–2101.
Taylor, D. B., 1996, ANISEIS V manual: Applied Geophysical Inc.
Thomsen, L. A., 1986, Weak elastic anisotropy: Geophysics, **51**, 1954–1966.
Tsvankin, I., 1995, Inversion of moveout velocities for horizontal transverse isotropy: 65th Ann. Internat. Mtg., Soc. Expl. Geophys., Expanded Abstracts, 735–738.
——— 1997, Reflection moveout and parameter estimation for horizontal transverse isotropy: Geophysics, **62**, 614–629.
Tsvankin, I., Grechka, V., and Cohen, J. K., 1997, Generalized Dix equation and modelling of normal moveout in inhomogeneous anisotropic media: 67th Ann. Internat. Mtg., Soc. Expl. Geophys., Expanded Abstracts, 1246–1249.

APPENDIX A

AZIMUTHAL MOVEOUT RESPONSE IN MULTILAYERED WEAKLY ANISOTROPIC HTI MEDIA

Consider multiazimuth seismic surveys over a stack of n HTI layers with arbitrary fracture orientation. I compute the traveltime, $t(\alpha, x)$, from the bottom of the nth layer for offset x and for the kth line azimuth at angle α from north. I then use this expression to derive the traveltime difference between two orthogonal lines for a fixed offset.

Traveltime equation

For the ith layer, I introduce the following azimuthally invariant interval properties: v_{p0i}, vertical P-wave velocity; t_{0i}, one-way zero-offset traveltime; ϵ_i and δ_i, Thomsen parameters; φ_i, fracture-strike azimuth from north. For the ray segment in the ith layer corresponding to the kth line azimuth, I use x_{ki} and θ_{ki} as the horizontal component and incidence angle of the ray segment, respectively, and t_{ki} as the traveltime along the ray segment. Thus, the total traveltime $t(\alpha, x)$ is

$$t(\alpha, x) = 2\sum_{i=1}^{n} t_{ki}, \tag{A-1}$$

where offset x satisfies

$$x = 2\sum_{i=1}^{n} x_{ki}. \tag{A-2}$$

Equation (A-2) implies that the ray is confined to the incidence plane and is valid only for weak azimuthalanisotropy.

From equation (5), t_{ki} can be written as

$$t_{ki} = \sqrt{t_{0i}^2 + \frac{x_{ki}^2}{v_{p0i}^2}\left[1 - (\delta_i - 2\epsilon_i)\sin^2\theta_{ki}\sin^2(\alpha - \varphi_i) - (\epsilon_i - \delta_i)\sin^4\theta_{ki}\sin^4(\alpha - \varphi_i)\right]}. \tag{A-3}$$

Similarly, introducing $t_{\|i}$ and $t_{\perp i}$ as the traveltime inside the ith layer for the survey lines parallel and perpendicular to the fracture strike of the ith layer, respectively, and $x_{\|i}$, $\theta_{\|i}$, $x_{\perp i}$ and $\theta_{\perp i}$ as the corresponding ray-segment components with the same total offset x gives

$$t_{\|i} = \sqrt{t_{0i}^2 + \frac{x_{\|i}^2}{v_{p0i}^2}} \tag{A-4}$$

and

$$t_{\perp i} = \sqrt{t_{0i}^2 + \frac{x_{\perp i}^2}{v_{p0i}^2}\left[1 - (\delta_i - 2\epsilon_i)\sin^2\theta_{\perp i} - (\epsilon_i - \delta_i)\sin^4\theta_{\perp i}\right]}. \quad \text{(A-5)}$$

Let

$$x_{ki} = x_{\parallel i}(1 + \nu_{ki}); \qquad \theta_{ki} = \theta_{\parallel i} + \Delta\theta_{ki}, \quad \text{(A-6)}$$

$$x_{\perp i} = x_{\parallel i}(1 + \nu_{\perp i}); \qquad \theta_{\perp i} = \theta_{\parallel i} + \Delta\theta_{\perp i}, \quad \text{(A-7)}$$

and ν_{ki} and $\nu_{\perp i}$ satisfy

$$\sum_{i=1}^{n} x_{\parallel i}\nu_{ki} = \sum_{i=1}^{n} x_{\parallel i}\nu_{\perp i} \equiv 0, \quad \text{(A-8)}$$

where ν_{ki}, $\Delta\theta_{ki}$, $\nu_{\perp i}$, and $\Delta\theta_{\perp i}$ are small quantities of the same order as the anisotropy parameters ϵ_i and δ_i. For weak anisotropy, higher orders of these terms can also be neglected in searching for linearized solutions. Substituting equation (A-6) into (A-3) and equation (A-7) into (A-5), then linearizing over the small quantities, gives

$$t_{ki} = t_{\parallel i} - t_{\parallel i}(\delta_i - 2\epsilon_i)\sin^2\theta_{\parallel i}\sin^2(\alpha - \varphi_i) - t_{\parallel i}(\epsilon_i - \delta_i)\sin^4\theta_{\parallel i}\sin^4(\alpha - \varphi_i) + \frac{\sin\theta_{\parallel i}}{v_{p0i}}x_{\parallel i}\nu_{ki} \quad \text{(A-9)}$$

and

$$t_{\perp i} = t_{\parallel i} - t_{\parallel i}(\delta_i - 2\epsilon_i)\sin^2\theta_{\parallel i} - t_{\parallel i}(\epsilon_i - \delta_i)\sin^4\theta_{\parallel i} + \frac{\sin\theta_{\parallel i}}{v_{p0i}}x_{\parallel i}\nu_{\perp i}. \quad \text{(A-10)}$$

This leads to

$$\begin{aligned} t(\alpha, x) = 2\sum_{i=1}^{n} t_{ki} = 2\sum_{i=1}^{n}\big[&t_{\parallel i}\cos^2(\alpha - \varphi_i) \\ &+ t_{\perp i}\sin^2(\alpha - \varphi_i)\big] + 2\sum_{i=1}^{n} t_{\parallel i}(\epsilon_i - \delta_i) \\ &\times \sin^4\theta_{\parallel i}\sin^2(\alpha - \varphi_i)\cos^2(\alpha - \varphi_i) \\ &- 2\sum_{i=1}^{n}\frac{\sin\theta_{\parallel i}}{v_{p0i}}x_{\parallel i}\nu_{\perp i}\sin^2(\alpha - \varphi_i) \\ &+ 2\sum_{i=1}^{n}\frac{\sin\theta_{\parallel i}}{v_{p0i}}x_{\parallel i}\nu_{ki}. \end{aligned} \quad \text{(A-11)}$$

Traveltime difference between orthogonal lines

Assume an orthogonal line at azimuth $\alpha + \pi/2$. In equation (A-11), ν_{ki} is the only variable that still implicitlyvaries with azimuth. Use ν'_{ki} to denote the corresponding value for the orthogonal line at azimuth $\alpha + \pi/2$. Using equation (A-11), the traveltime difference Δt between the two orthogonal lines can be written as

$$\begin{aligned} \Delta t(\alpha, x) &= t(\alpha + \pi/2, x) - t(\alpha, x) \\ &= 2\sum_{i=1}^{n}\left(t_{\perp i} - t_{\parallel i} - \frac{\sin\theta_{\parallel i}}{v_{p0i}}x_{\parallel i}\nu_{\perp i}\right) \\ &\quad \times \cos 2(\alpha - \varphi_i) + 2\sum_{i=1}^{n}\frac{\sin\theta_{\parallel i}}{v_{p0i}}x_{\parallel i}(\nu'_{ki} - \nu_{ki}). \end{aligned} \quad \text{(A-12)}$$

To the first order in the small anisotropy quantities,

$$\sum_{i=1}^{n}\frac{\sin\theta_{\parallel i}}{v_{p0i}}x_{\parallel i}(\nu'_{ki} - \nu_{ki}) = p\sum_{i=1}^{n} x_{\parallel i}(\nu'_{ki} - \nu_{ki}) \equiv 0,$$

where p is the horizontal slowness (ray parameter). Using equation (A-10) yields

$$\Delta t(\alpha, x) = \sum_{i=1}^{n} B_i(\epsilon_i, \delta_i, x_{\parallel i})\cos 2(\alpha - \varphi_i), \quad \text{(A-13)}$$

where

$$B_i(\epsilon_i, \delta_i, x_{\parallel i}) = \frac{2x_{\parallel i}}{v_{p0i}}\sin\theta_{\parallel i}\left[2\epsilon_i - \delta_i - (\epsilon_i - \delta_i)\sin^2\theta_{\parallel i}\right]. \quad \text{(A-14)}$$

For the special case of multilayered media with a uniform fracture-strike azimuth $\varphi_i \equiv \varphi$, equation (A-13) becomes

$$\begin{aligned} \Delta t(\alpha, x) &= 2\cos 2(\alpha - \varphi)\sum_{i=1}^{n}(t_{\perp i} - t_{\parallel i}) \\ &\quad - 2p\cos 2(\alpha - \varphi)\sum_{i=1}^{n} x_{\parallel i}\nu_{\perp i} \\ &= (t_\perp - t_\parallel)\cos 2(\alpha - \varphi), \end{aligned} \quad \text{(A-15)}$$

which reduces to equation (13).